Binary small molecule organic nanoparticles exhibit both direct and diffusion-limited ultrafast charge transfer with NIR excitation

Bryan Kudisch[1], Margherita Maiuri[1], Leon Wang[2], Tristan Lim[2], Hoang Lu[2], Victoria Lee[2], Robert K. Prud'homme[2], Gregory D. Scholes[1*]

[1]Department of Chemistry, Princeton University, Princeton, NJ 08544, USA.

[2]Department of Chemical and Biological Engineering, Princeton University, Princeton, NJ 08544, USA.

S1. Tabulated formulations for QDI, VONc, and Binary NPs

Nanoparticle	QDI loading (mg/mL)	VONc loading (mg/mL)	PS-b-PEG loading (mg/mL)	PS loading (mg/mL)
QDI only	5	-	5	-
VONc only	-	5	5	-
Binary 1	5	1.25	5	-
Binary 2	2.5	5	5	-
Binary 3	1.25	5	5	-
Binary 1 plus 10 mg/mL PS	5	1.25	5	10
Binary 1 plus 20 mg/mL PS	5	1.25	5	20

S2. Dynamic light scattering of QDI, VONc, and Binary 1 Nanoparticles Prepared by Flash Nanoprecipitation

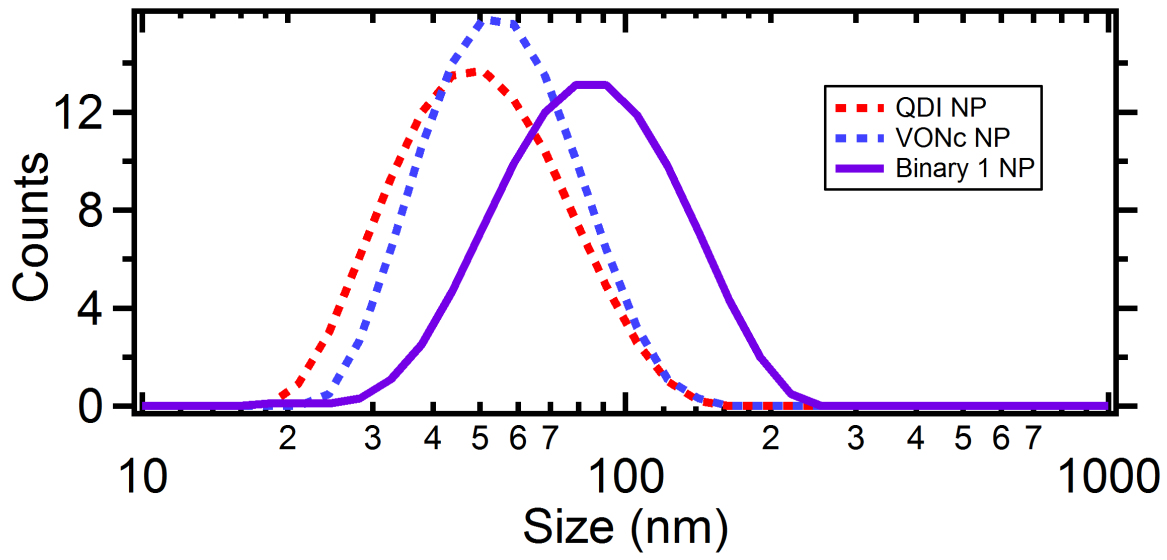

S3. TEM image of VONc NP

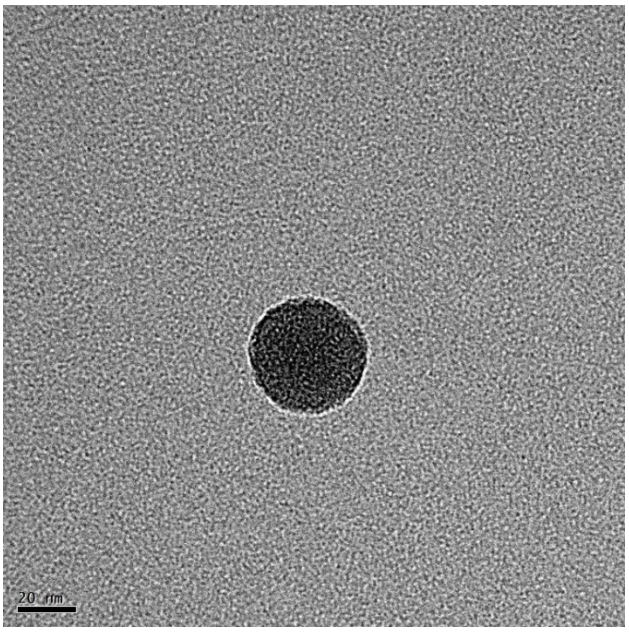

S4. TEM image of representative QDI nanoparticle, as well as a cluster of QDI nanoparticles.

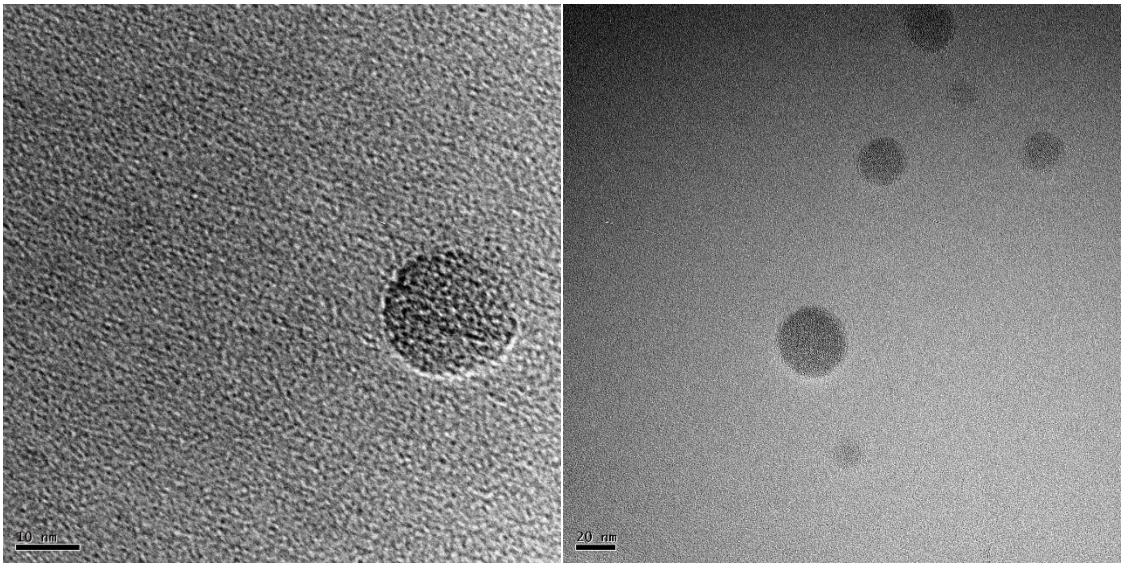

S5. TEM image of a representative binary nanoparticle, with the formulation of Binary 1. A TEM diffractogram of this nanoparticle is also including, which shows that there is relatively no crystallinity in this nanoparticle, as it shows no diffraction rings.

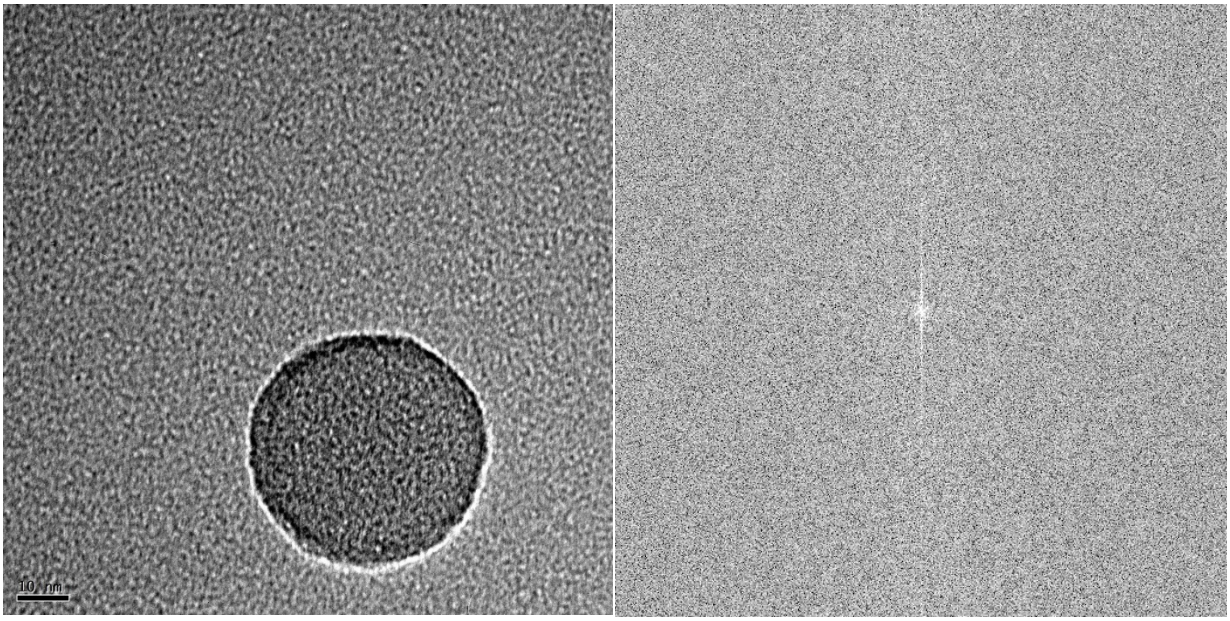

S6. Normalized absorption and emission spectrum of QDI in toluene solution.

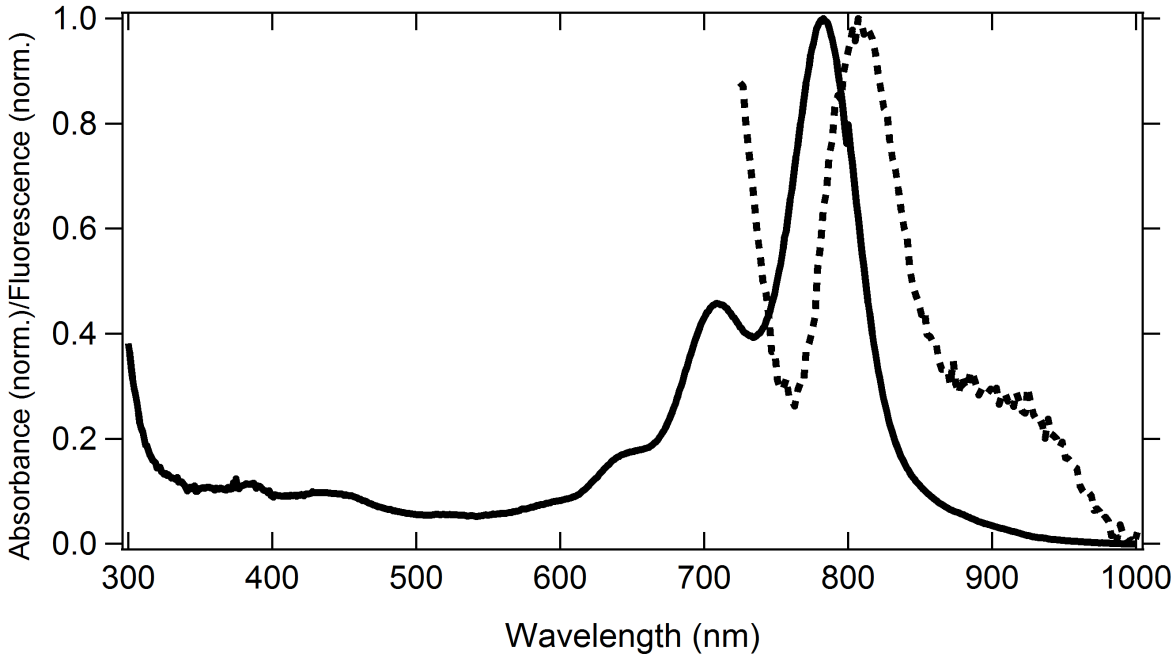

S7. Normalized absorption with attempted fluorescence measurement of a QDI NP.

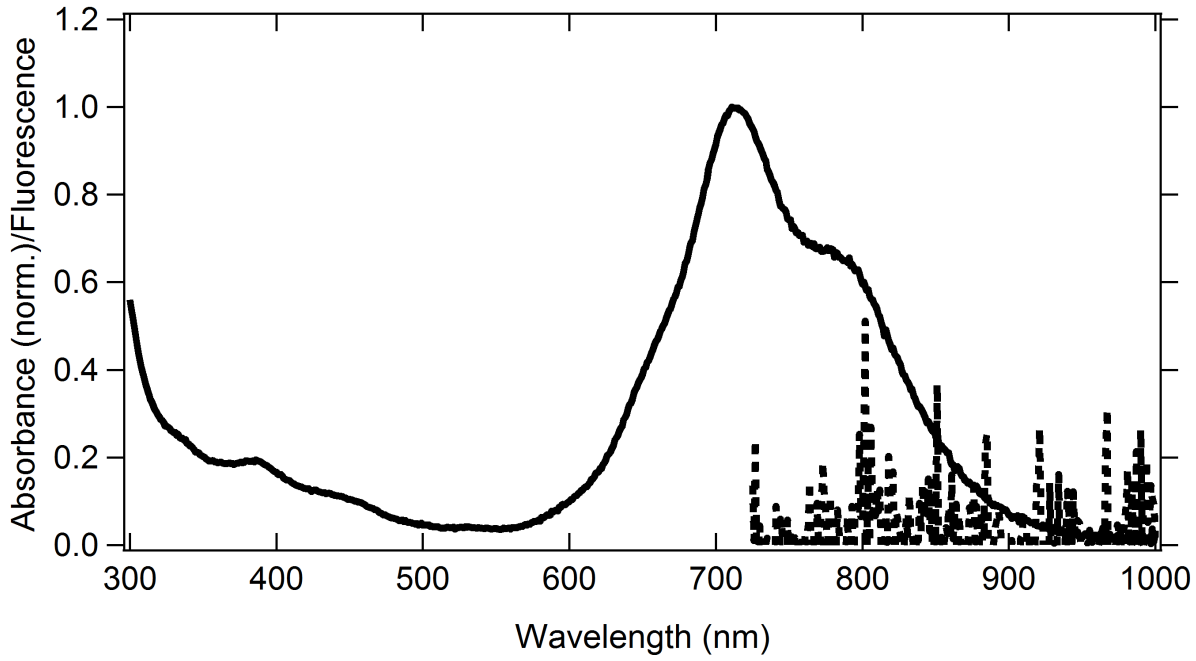

S8. Normalized absorption and attempted fluorescence of VONc NP.

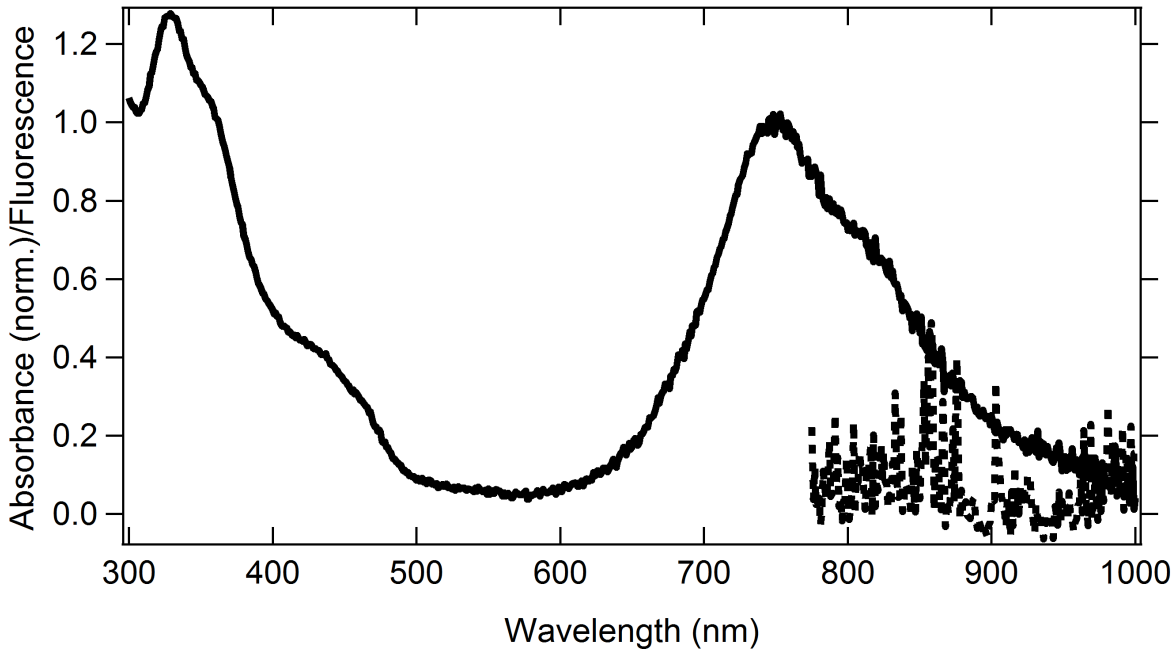

S9. Normalized absorption and attempted fluorescence of Binary 1.

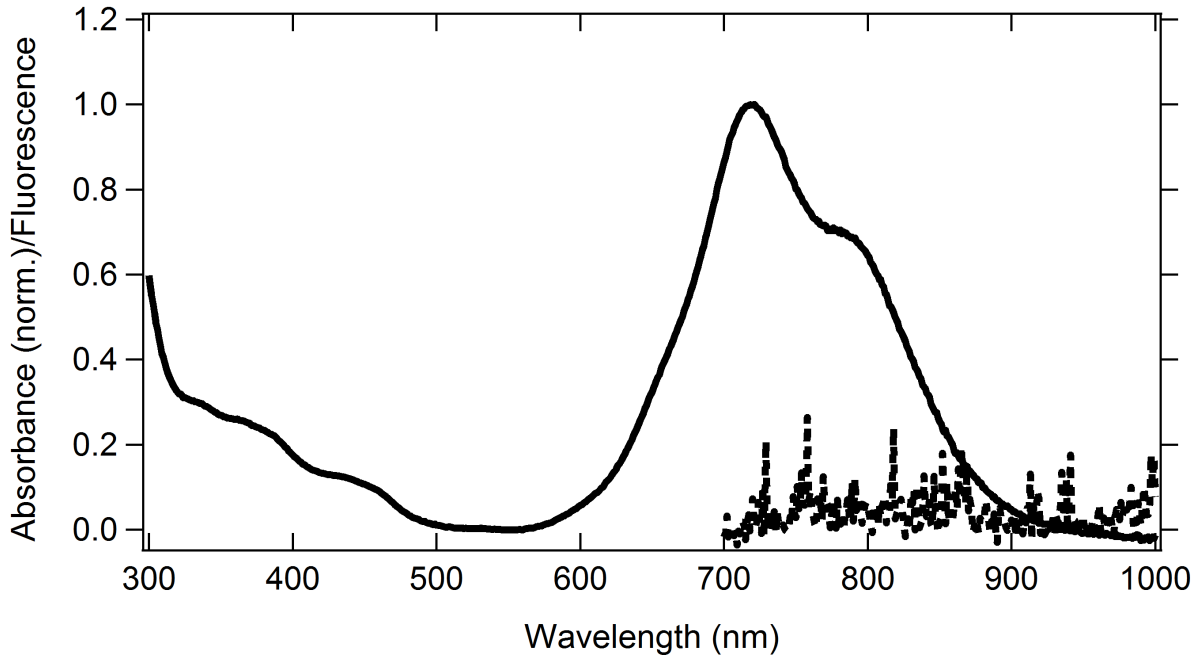

S10. Normalized absorption spectrum of a binary nanoparticle batch of Binary 1 compared to a mixture of QDI and VONc nanoparticles, intentionally composed such that the mixture reproduces the absorption spectrum of the Binary 1 system.

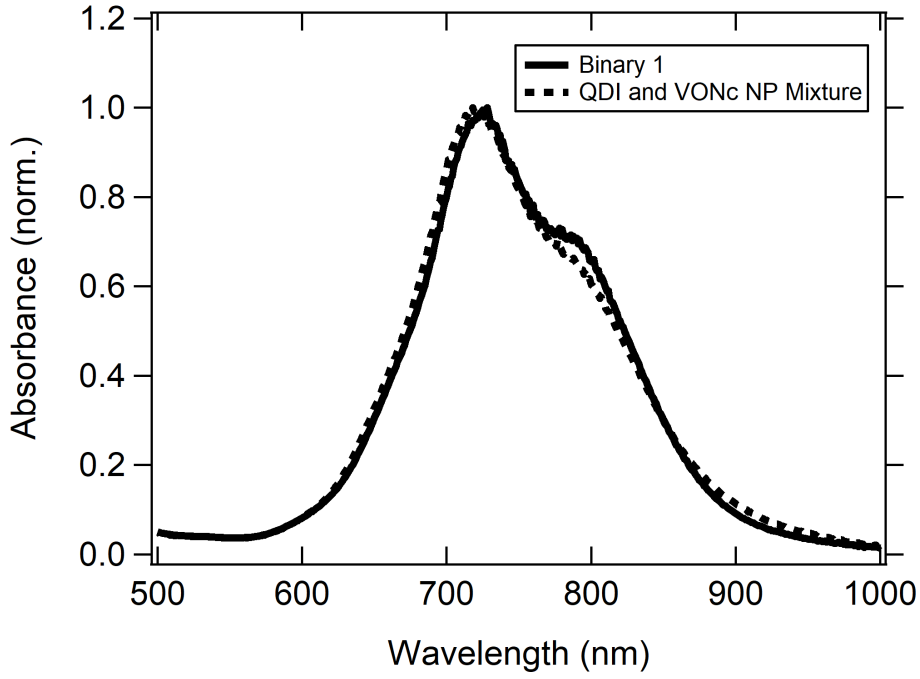

S11. Kinetics at 710 nm after photoexcitation at 620 nm at 15 uW pump power.

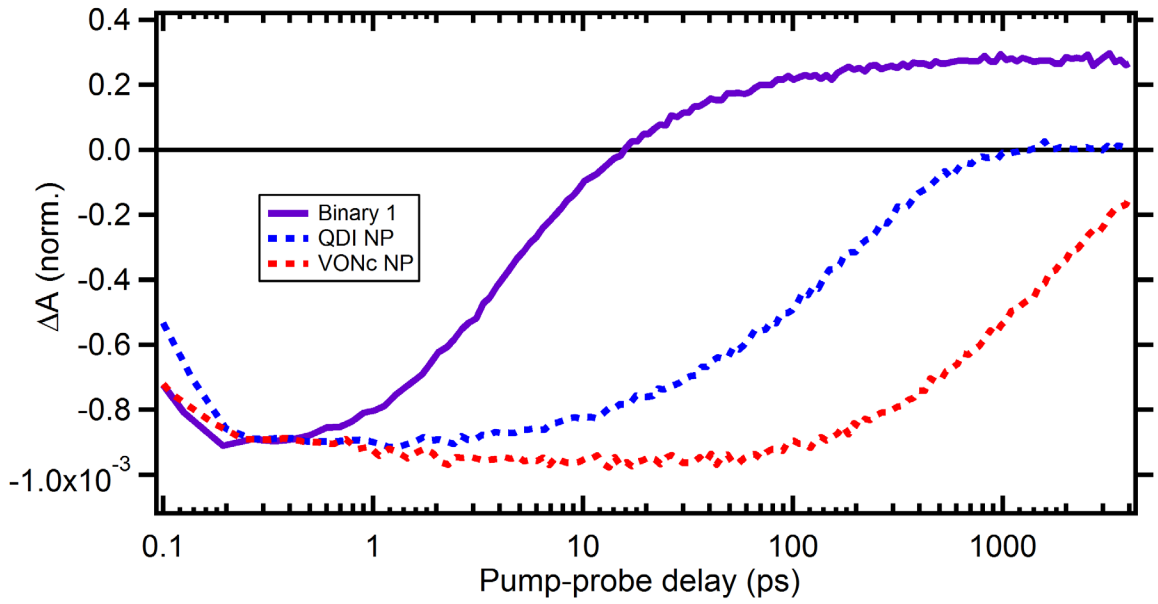

S12. 2D pump probe map of QDI in toluene solution after photoexcitation at 780 nm with 100 uW pump power.

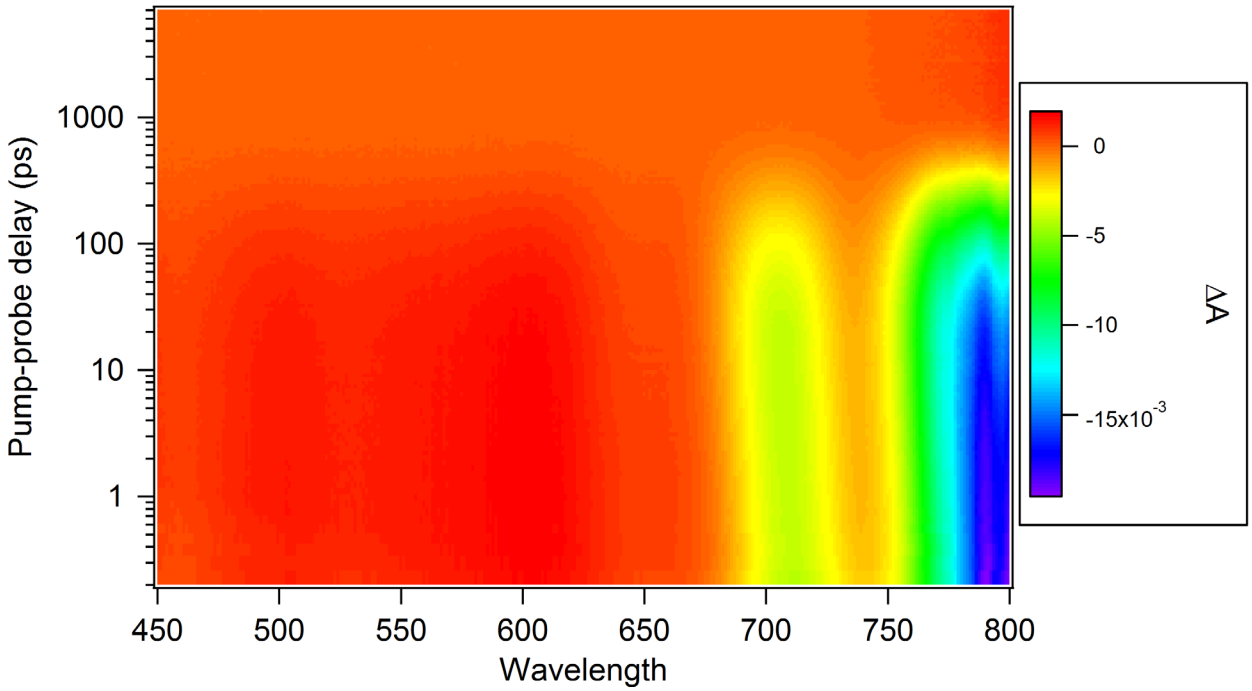

S13. Global analysis of QDI in toluene solution after photoexcitation at 780 nm with 100 uW pump power, using a 2-level sequential model.

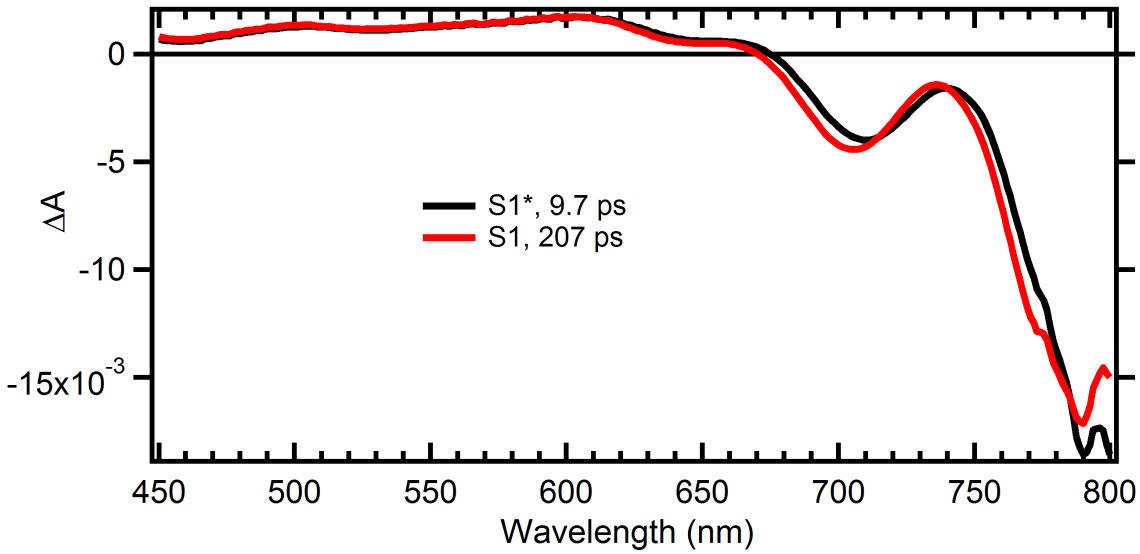

S14. Pump-probe kinetics of the QDI in toluene solution at 600 nm after photoexcitation at 780 nm with 100 uW pump power, overlayed with a single wavelength trace from the global fit

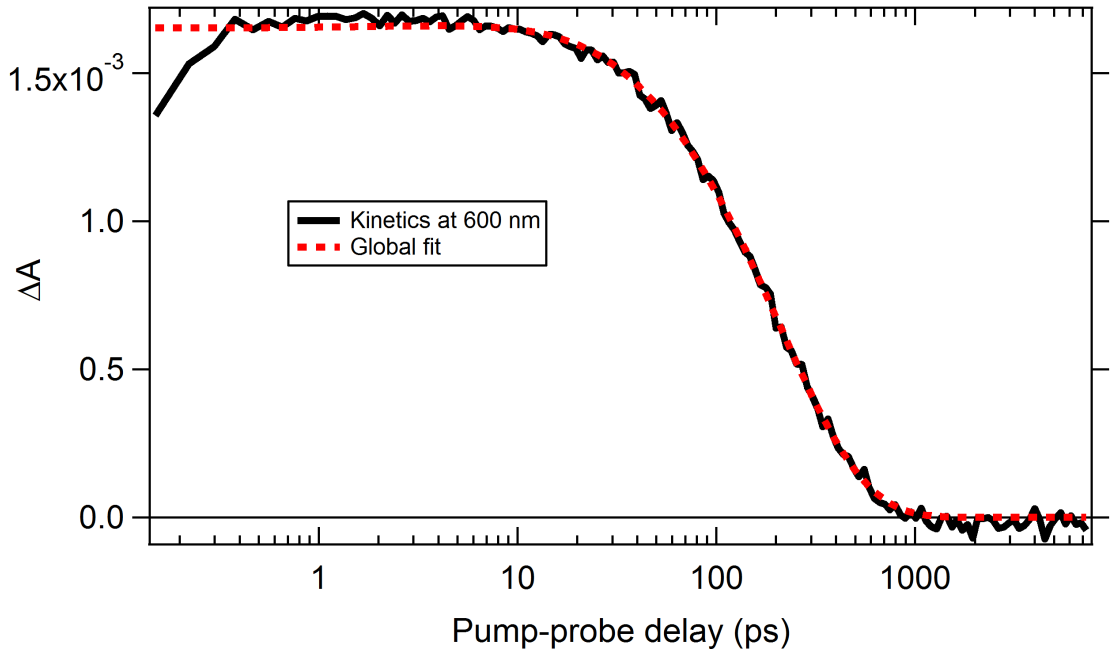

S15. Residual of the above fit with respect to the experimental kinetics

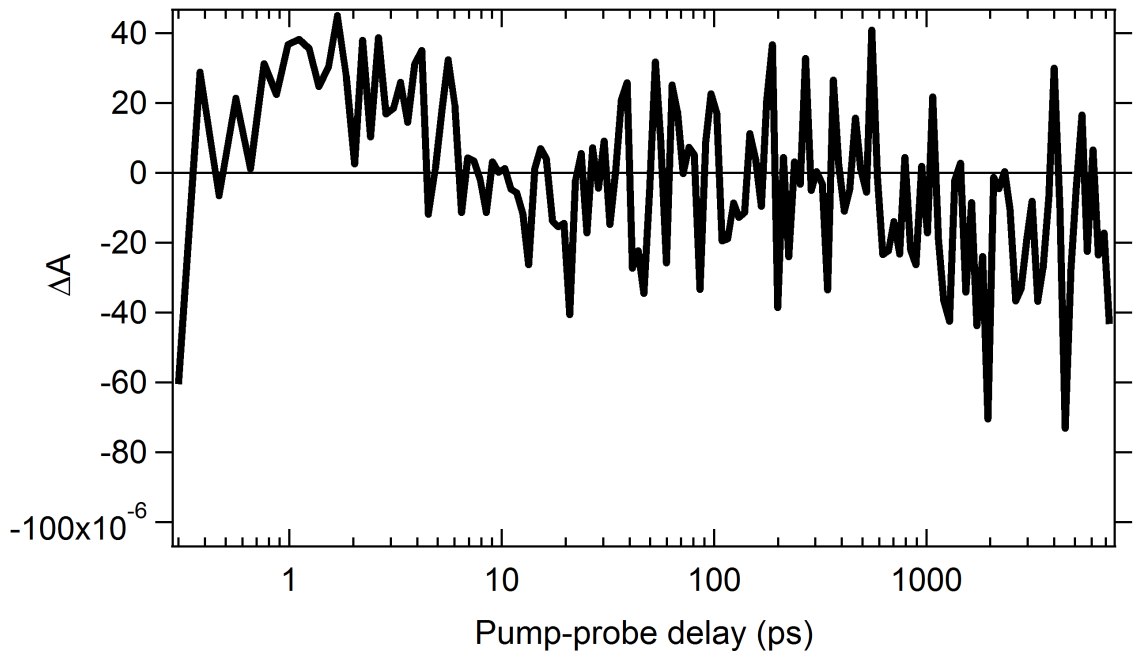

S16. Pump-probe kinetics of the QDI in toluene solution at 770 nm after photoexcitation at 780 nm with 100 uW pump power, overlayed with a single wavelength trace from the global fit.

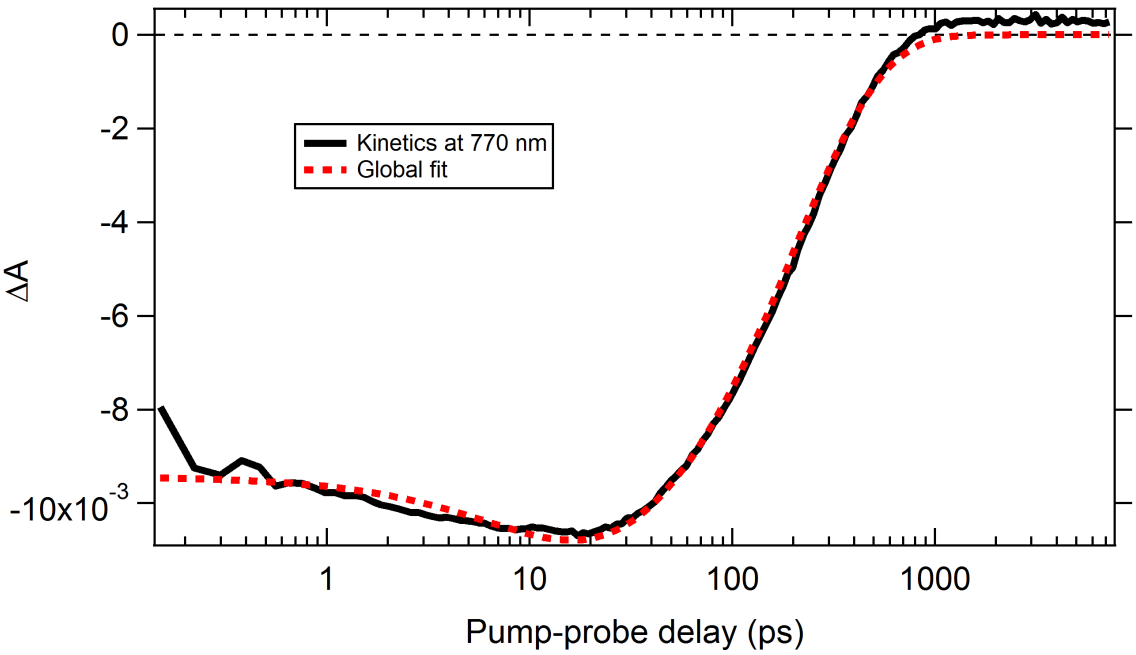

S17. Residual of the above fit with respect to the experimental kinetics

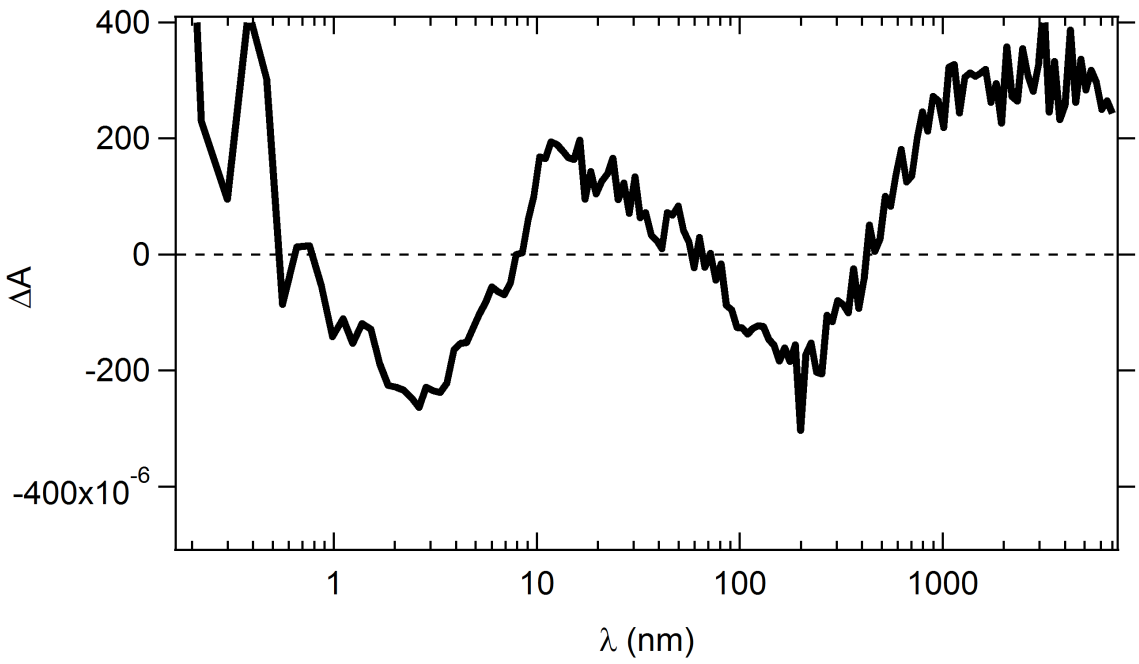

S18. 2D pump probe map of the QDI NP solution after photoexcitation at 620 nm with 5 uW pump power.

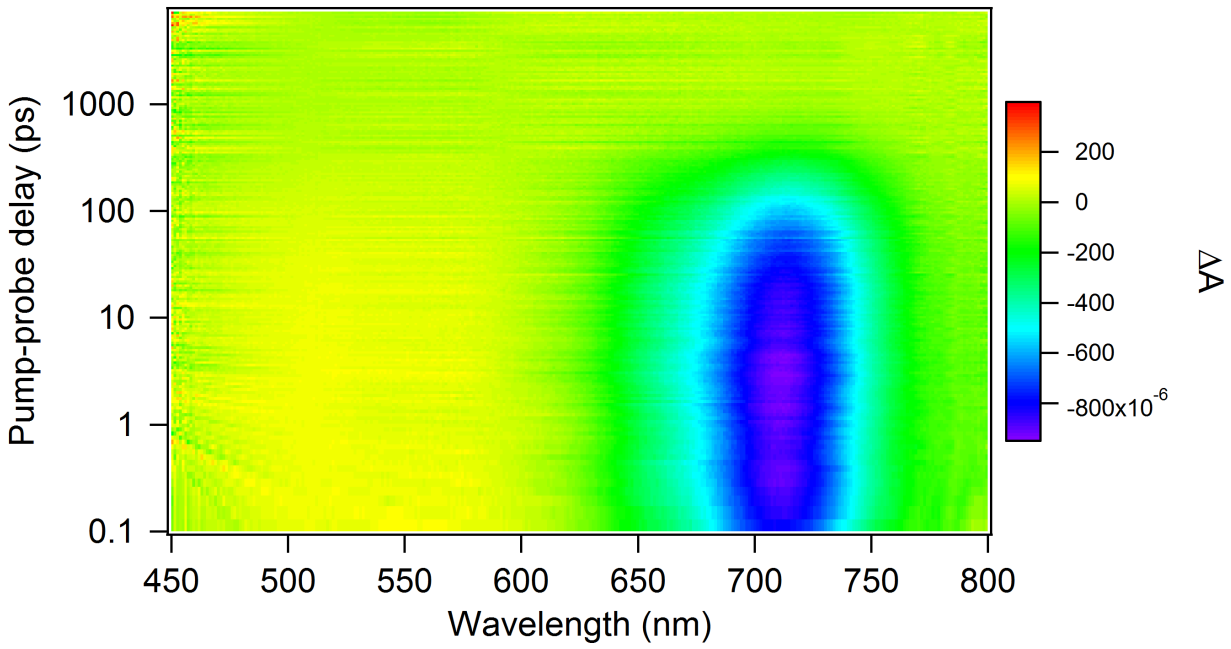

S19. Pump-probe kinetics of the QDI NP solution at 562 nm after photoexcitation at 620 nm with 5 uW pump power, overlayed with a single wavelength trace from the global fit.

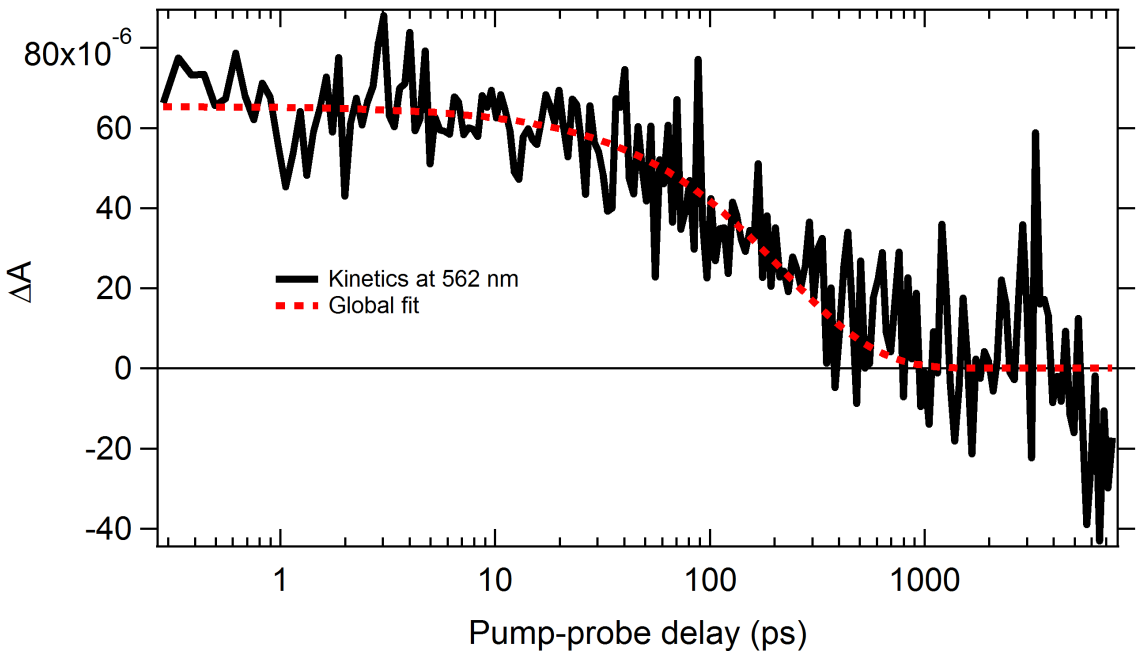

S20. Residual of the above fit with respect to the experimental kinetics

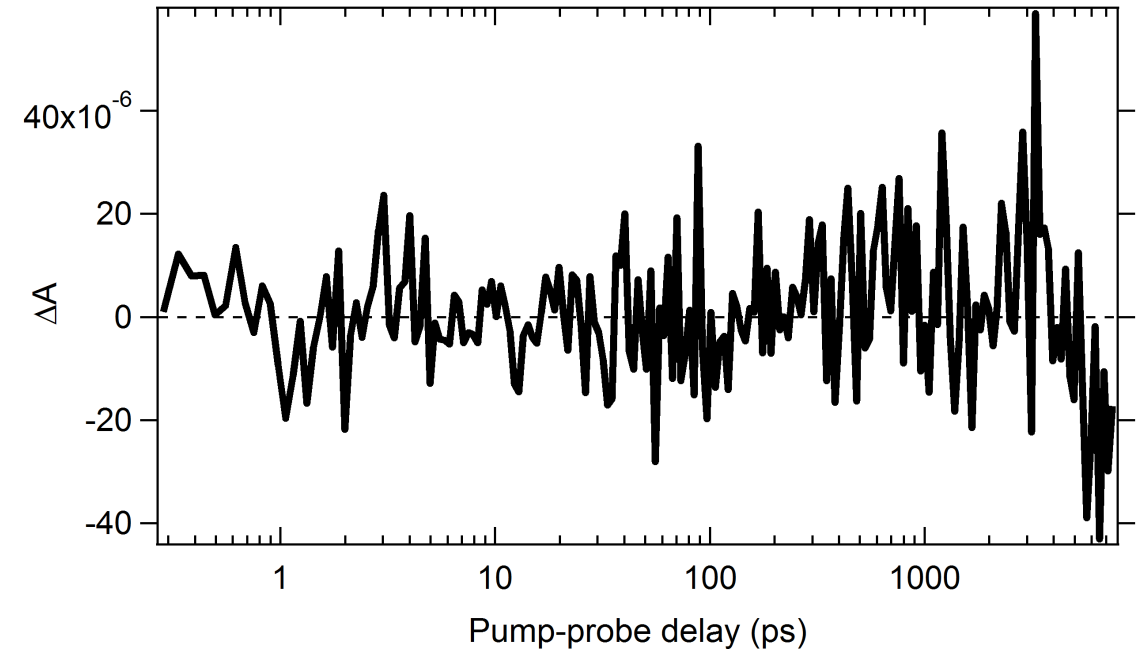

S21. Power dependent kinetics of the QDI NP solution showing finite singlet-singlet annihilation at pump powers large than 15 uW following photoexcitation at 620 nm

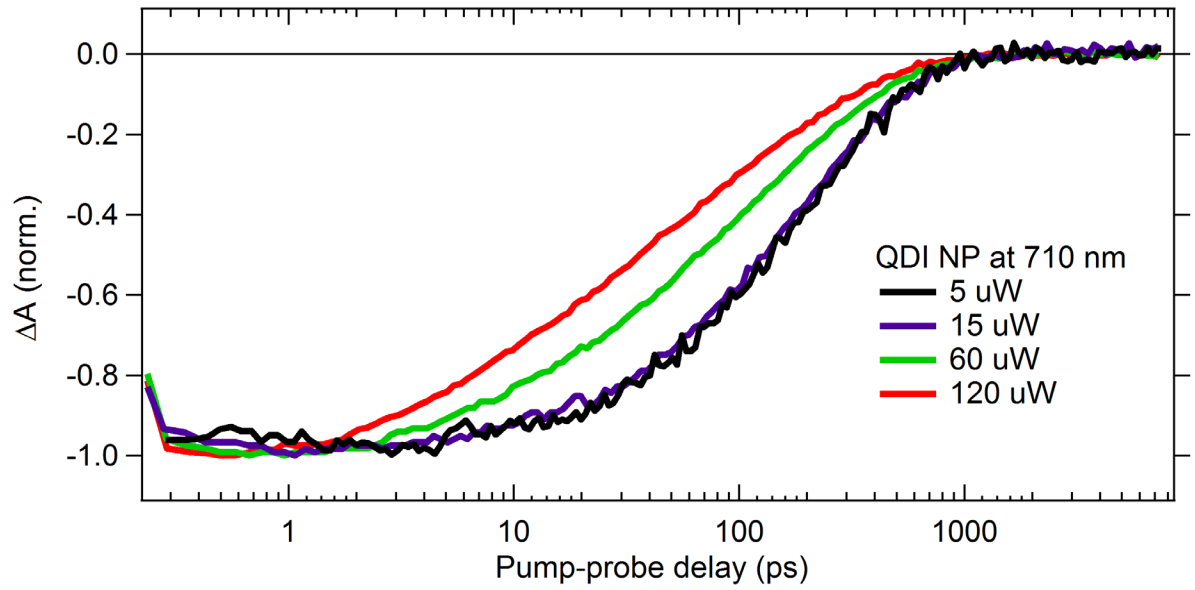

S22. 2D pump probe map of VONc in toluene solution after photoexcitation at 810 nm with 100 uW pump power.

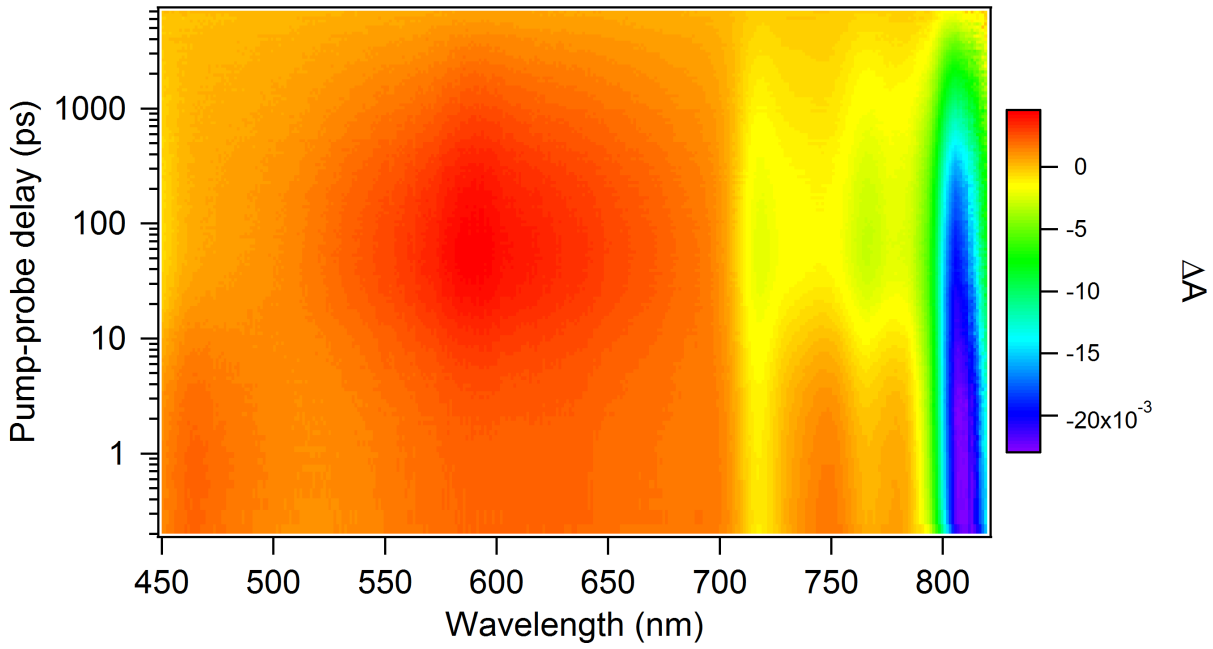

S23. Global analysis of VONc in toluene solution after photoexcitation at 810 nm with 100 uW pump power, using a 2-level sequential model.

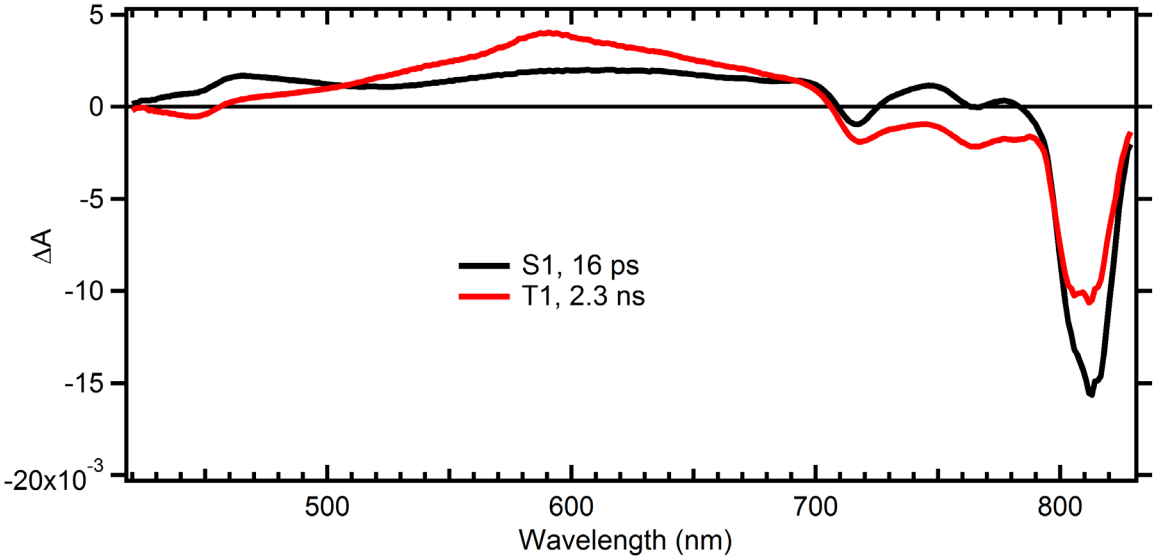

S24. Pump-probe kinetics of the VONc in toluene solution at 590 nm after photoexcitation at 810 nm with 100 uW pump power, overlayed with a single wavelength trace from the global fit.

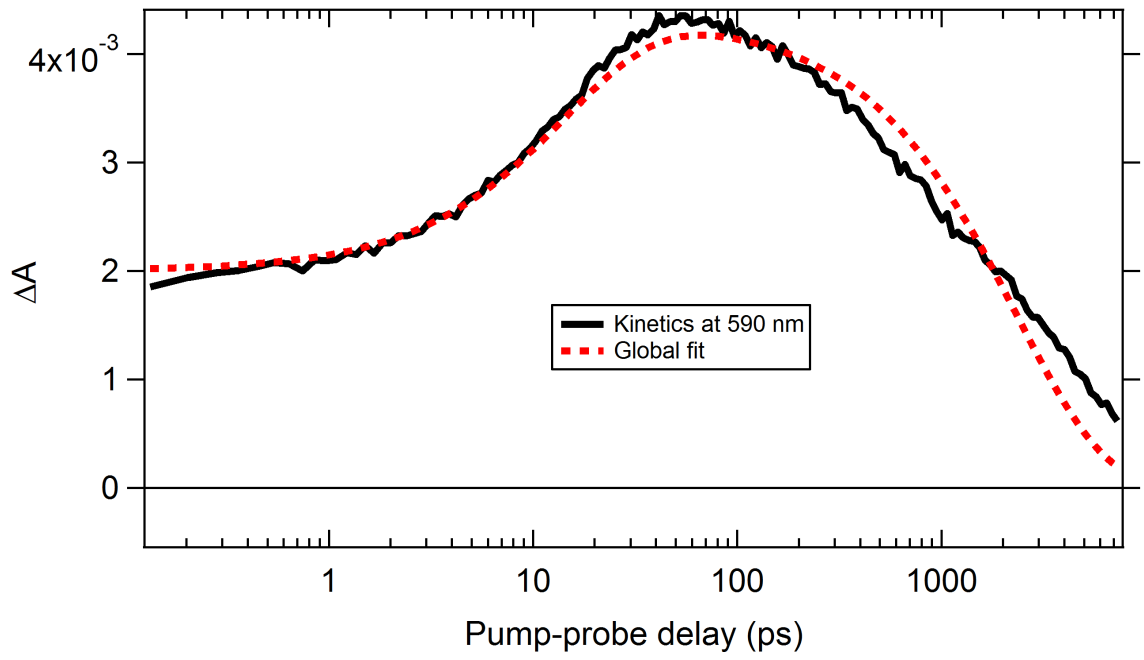

S25. Residual of the above fit with respect to the experimental kinetics

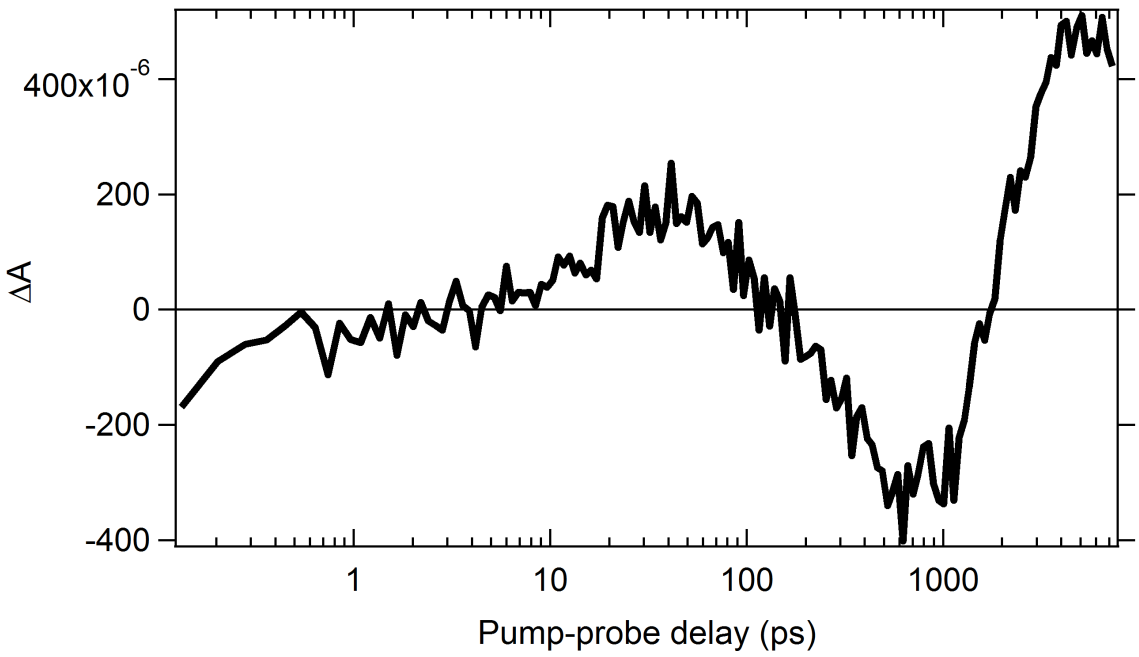

S26. Pump-probe kinetics of the VONc in toluene solution at 808 nm after photoexcitation at 810 nm with 100 uW pump power, overlayed with a single wavelength trace from the global fit.

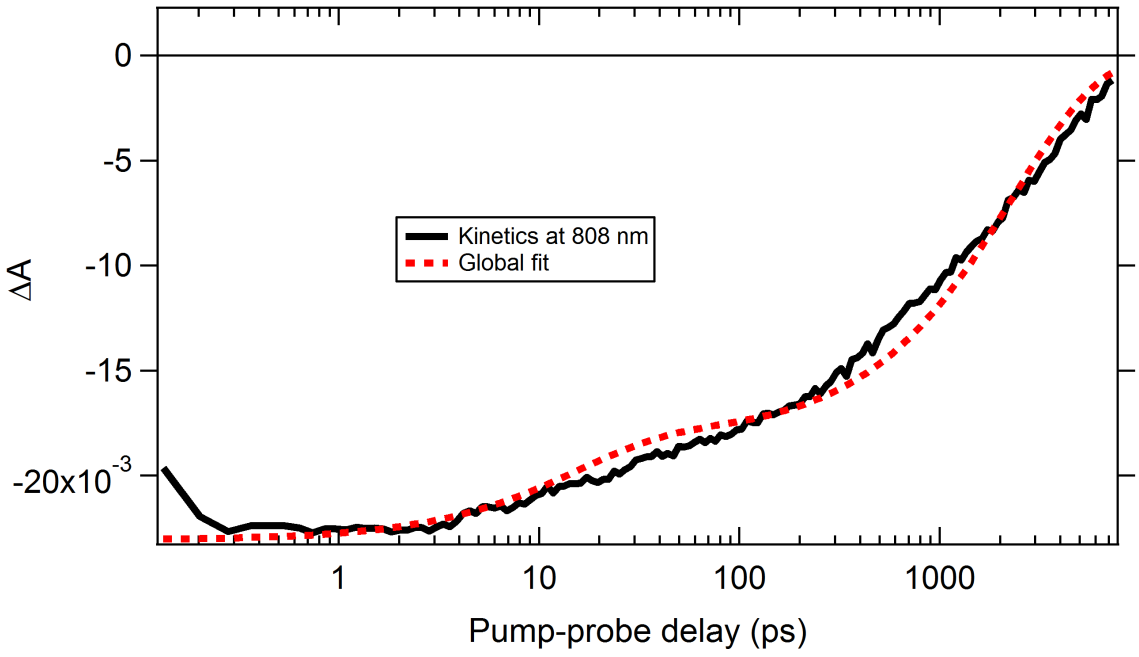

S27. Residual of the above fit with respect to the experimental kinetics.

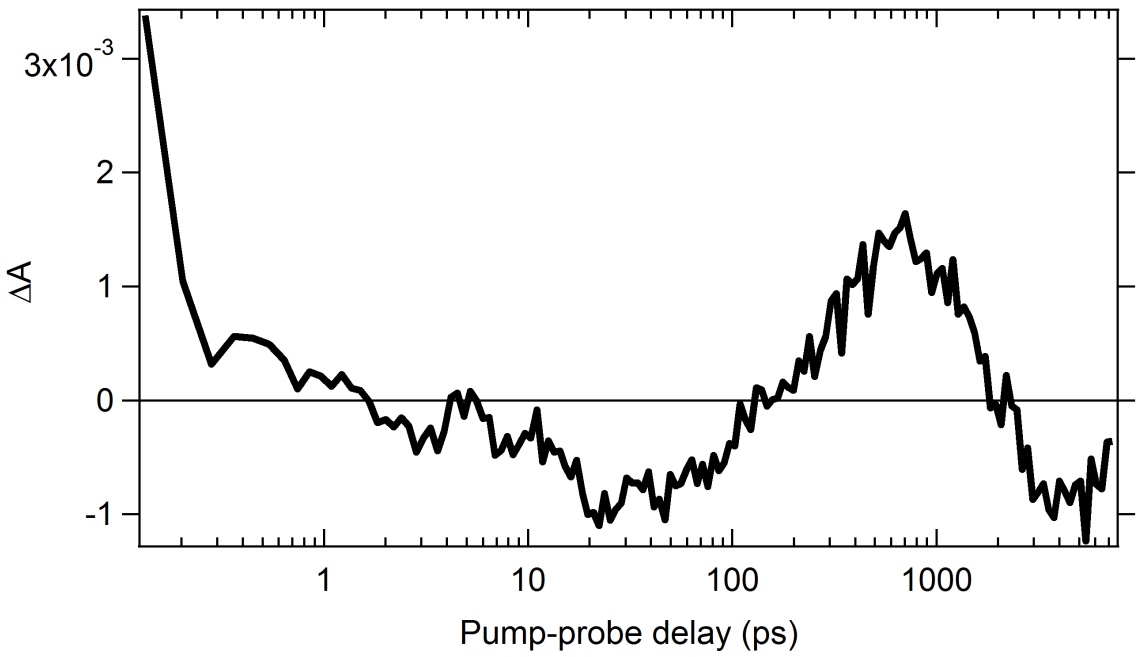

S28. 2D pump probe map of the VONc NP solution after photoexcitation at 620 nm with 20 uW pump power.

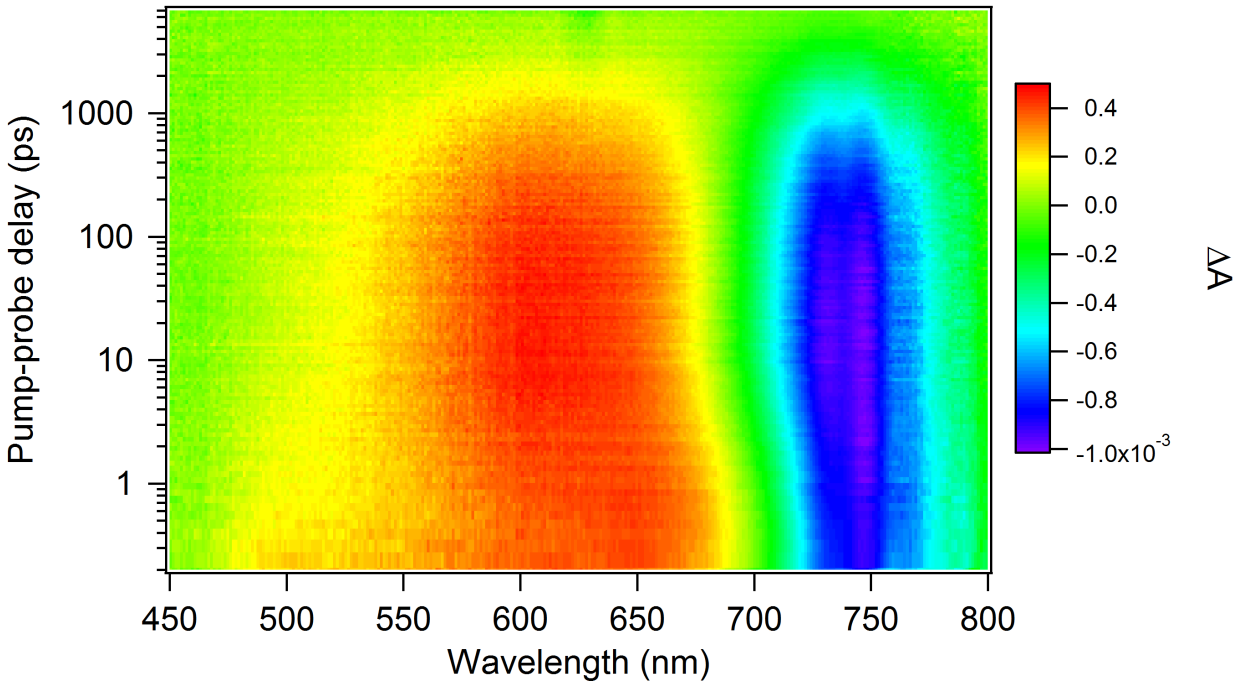

S29. Pump-probe kinetics of the VONc NP solution at 612 nm after photoexcitation at 620 nm with 20 uW pump power, overlayed with a single wavelength trace from the global fit.

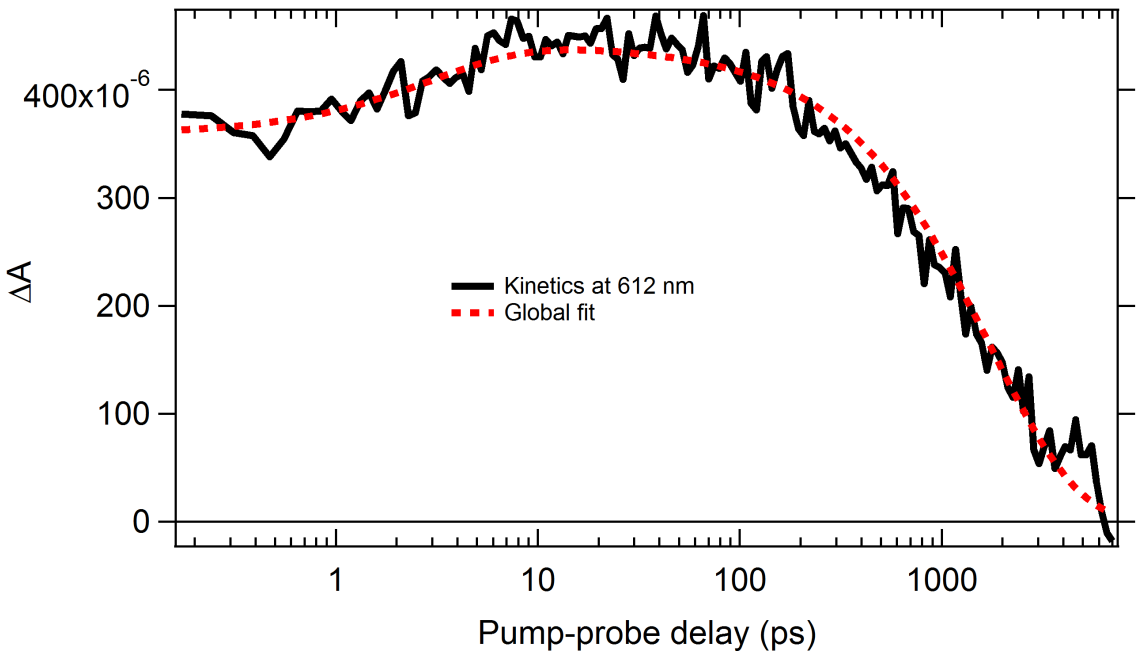

S30. Residual of the above fit with respect to the experimental kinetics.

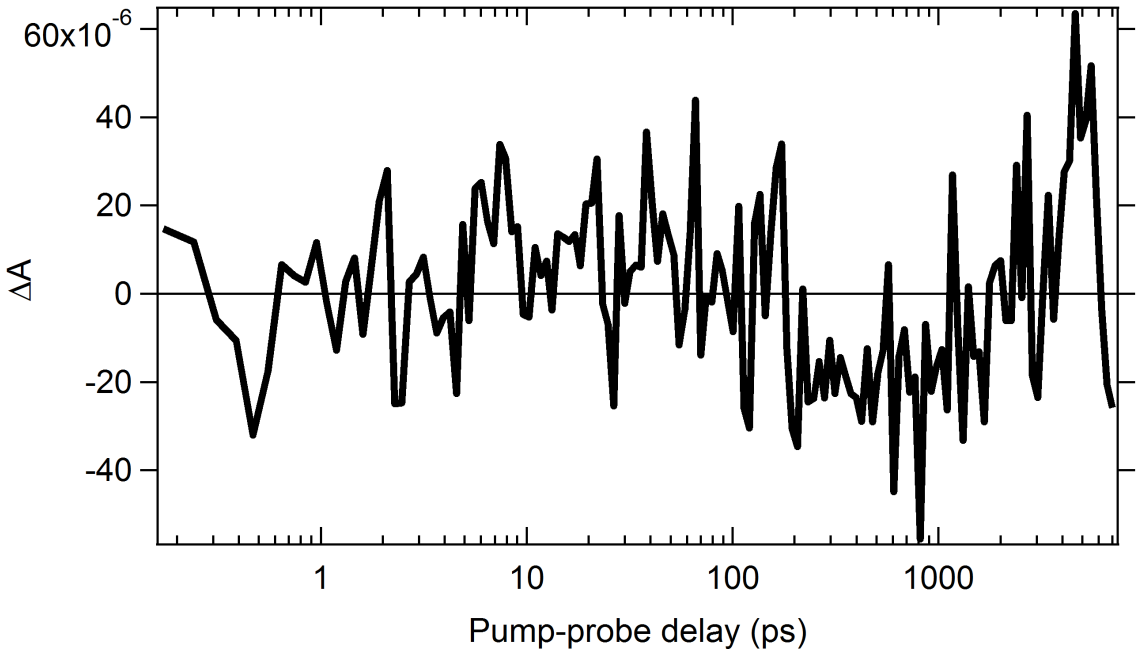

S31. Pump-probe kinetics of the VONc NP solution at 612 nm after photoexcitation at 620 nm with 20 uW pump power, overlaid with a single wavelength trace from the global fit.

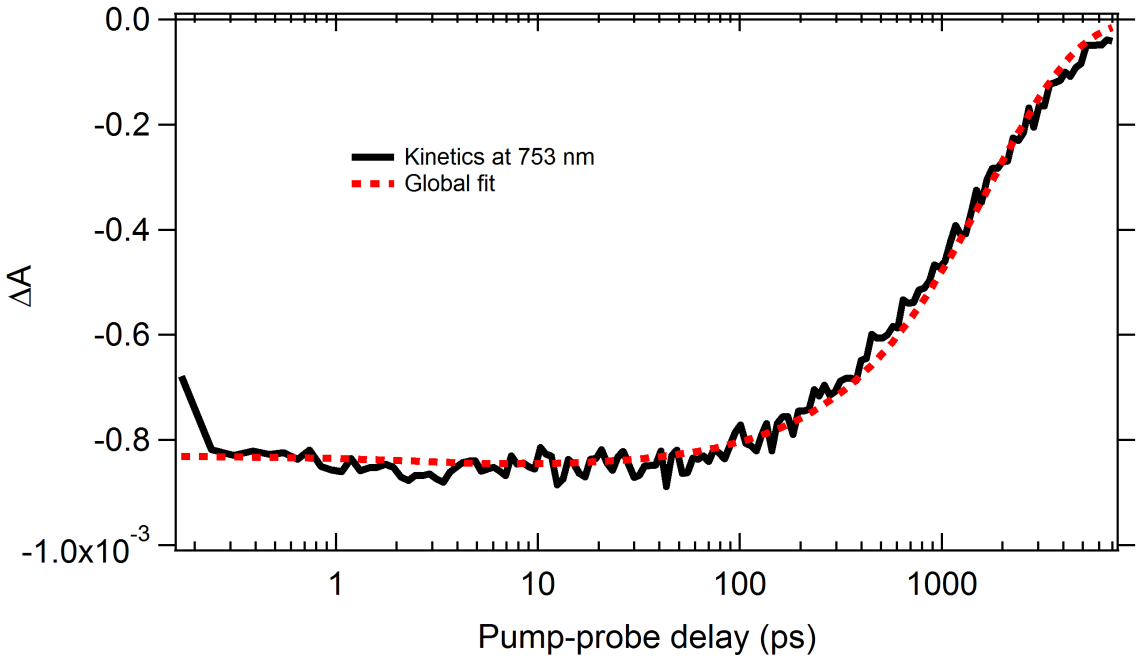

S32. Residual of the above fit with respect to the experimental kinetics.

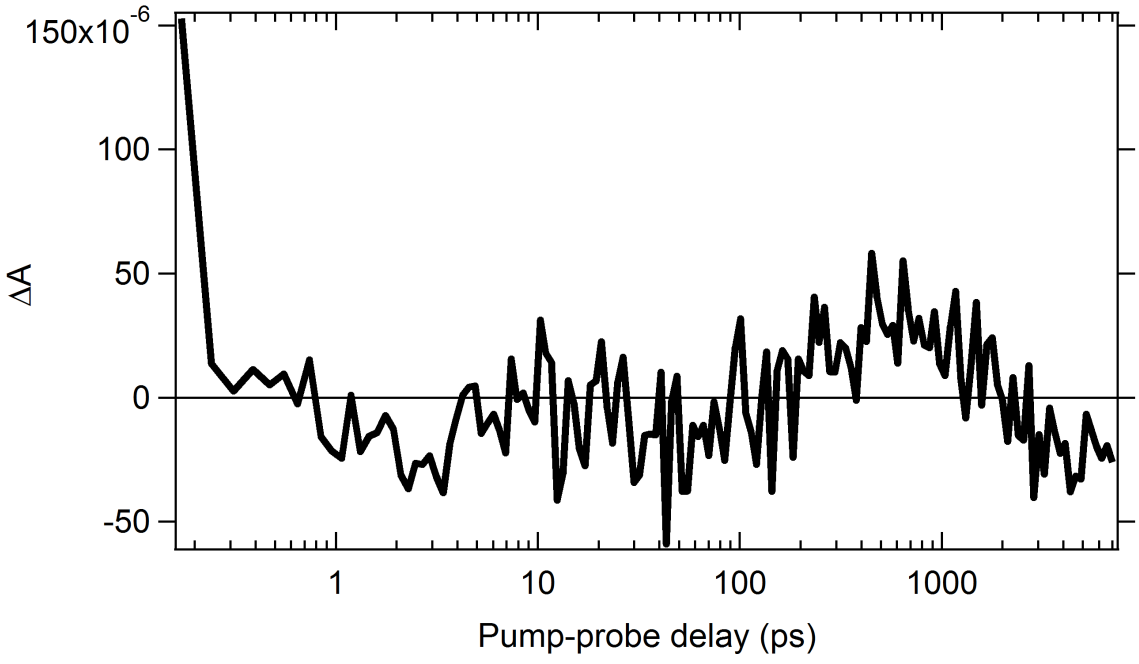

S33. 2D pump probe map of the Binary 1 NP solution after photoexcitation at 710 nm with 5 uW pump power.

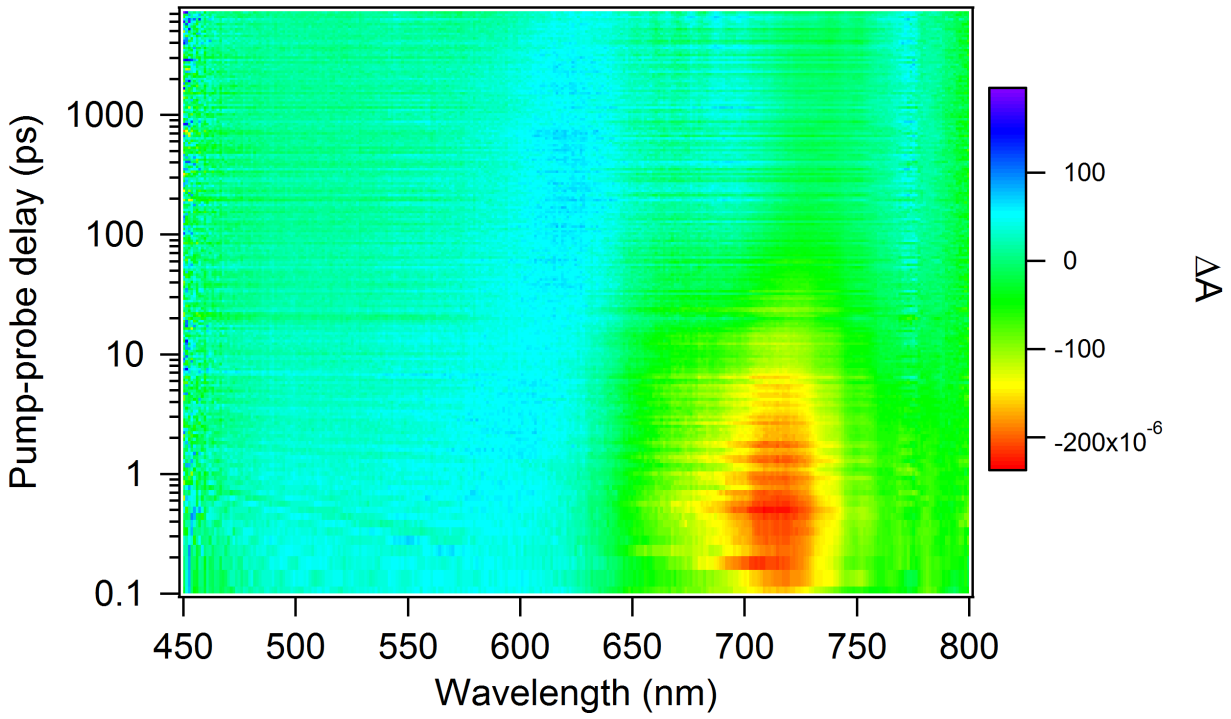

S34. Pump-probe kinetics of the Binary 1 NP solution at 627 nm after photoexcitation at 710 nm with 5 uW pump power, overlayed with a single wavelength trace from the global fit.

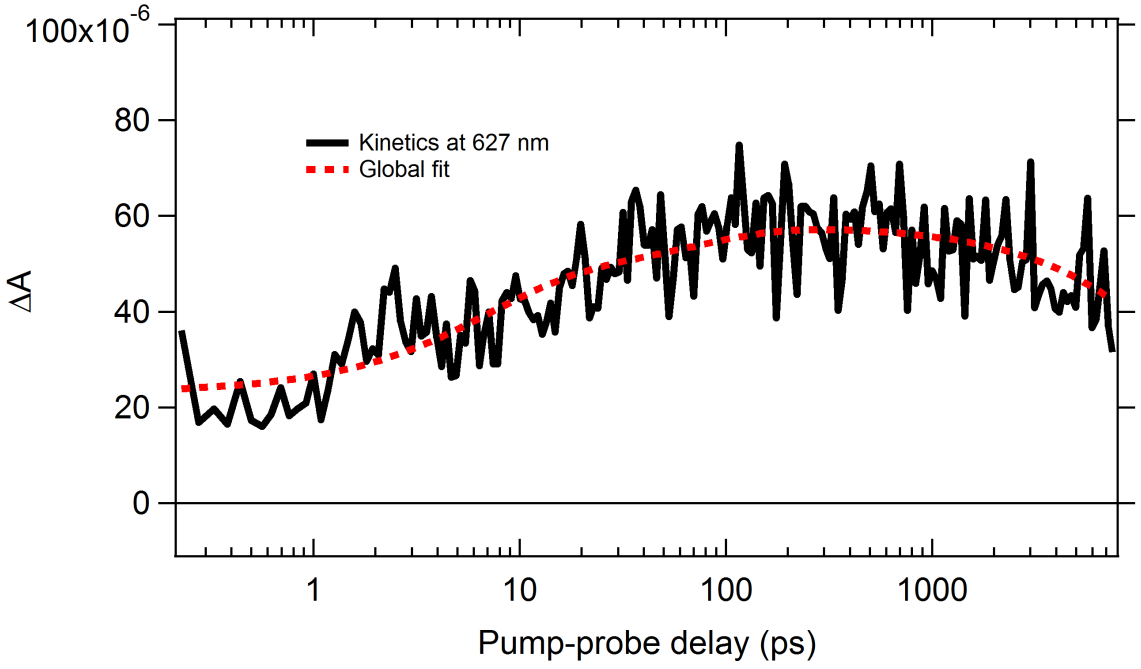

S35. Residual of the above fit with respect to the experimental kinetics.

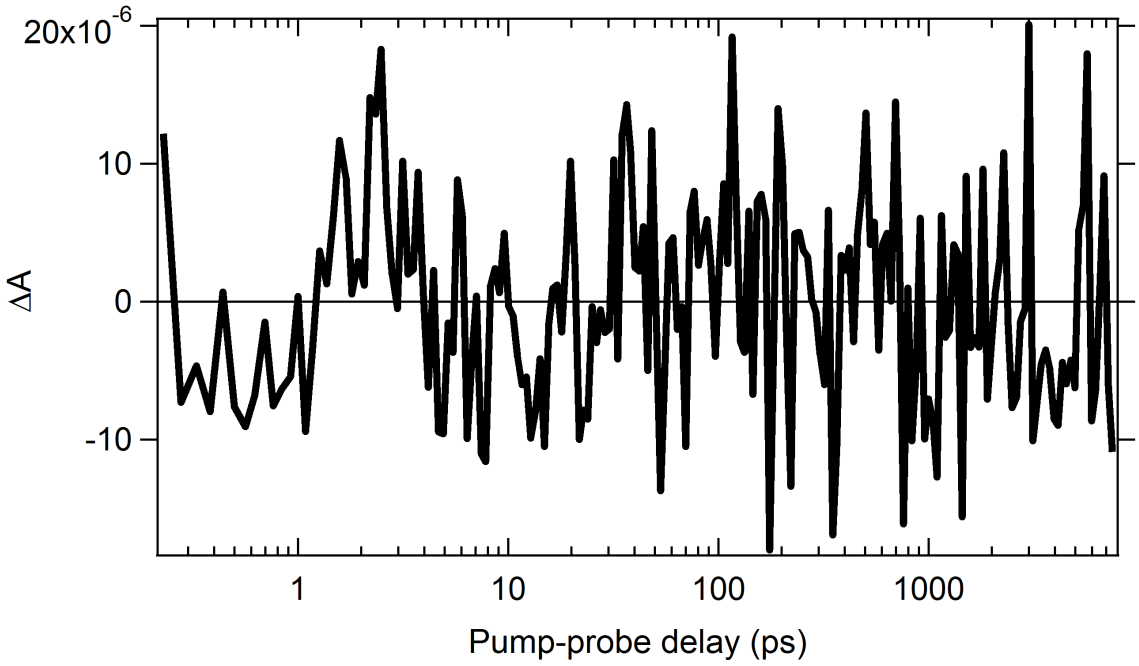

S36. Pump-probe kinetics of the Binary 1 NP solution at 688 nm after photoexcitation at 710 nm with 5 uW pump power, overlayed with a single wavelength trace from the global fit.

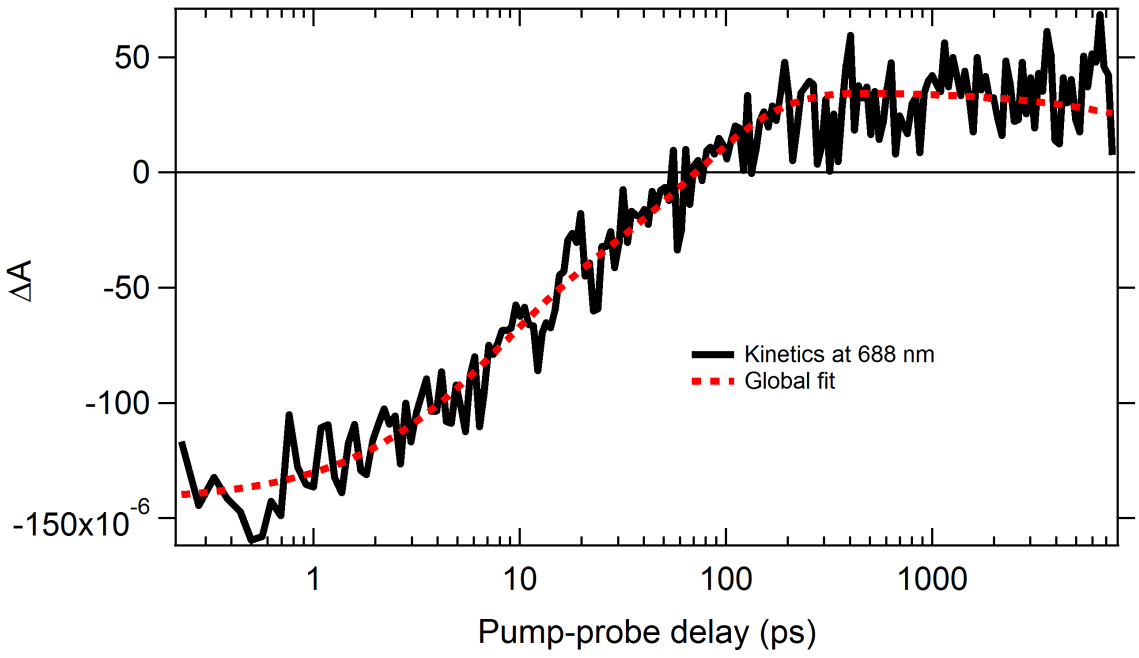

S37. Residual of the above fit with respect to the experimental kinetics.

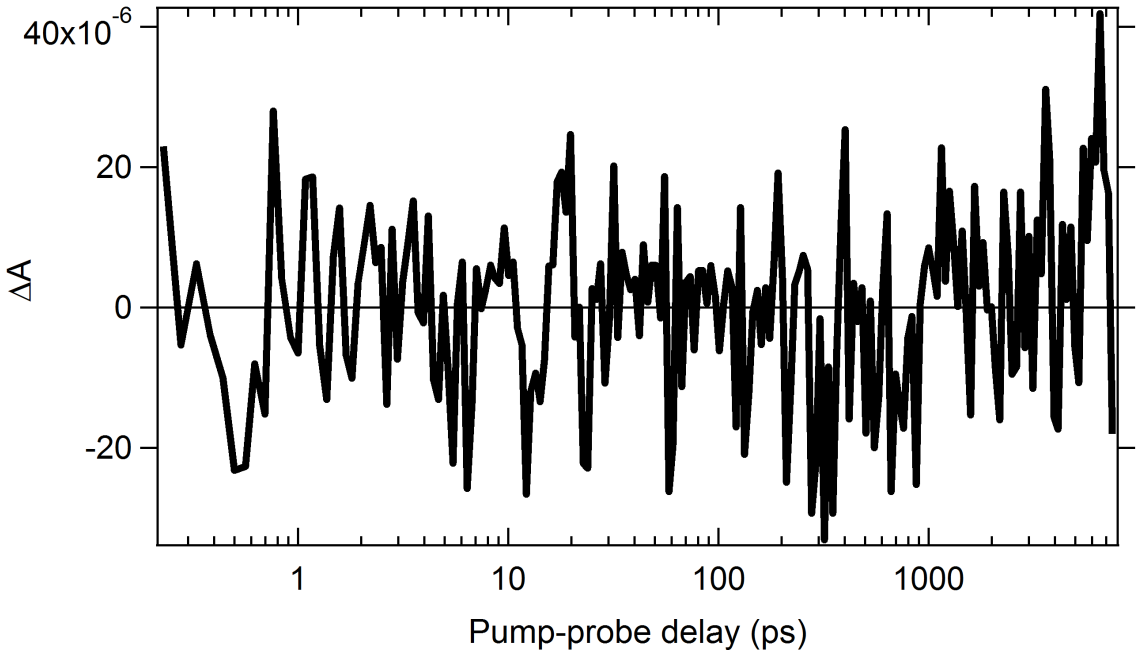

S38. Global analysis of the Binary 1 NP solution after photoexcitation at 710 nm with 5 uW pump power, using a 2-level sequential model.

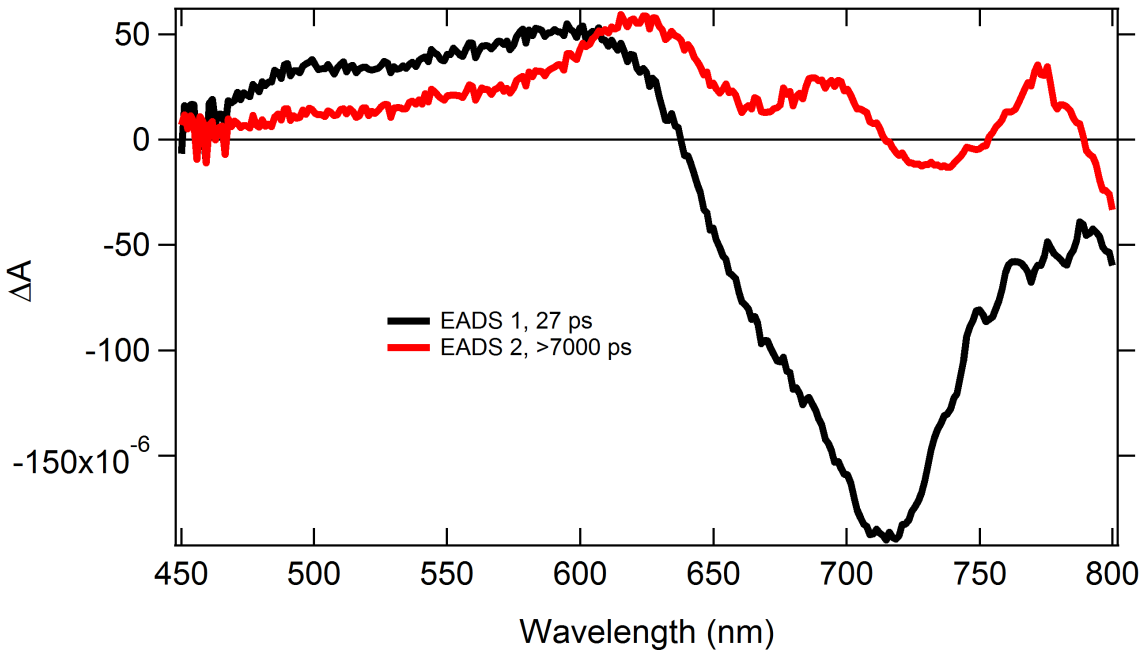

S39. Pump-probe kinetics of the Binary 1 NP solution at 627 nm after photoexcitation at 710 nm with 5 uW pump power, overlayed with a single wavelength trace from the above global fit.

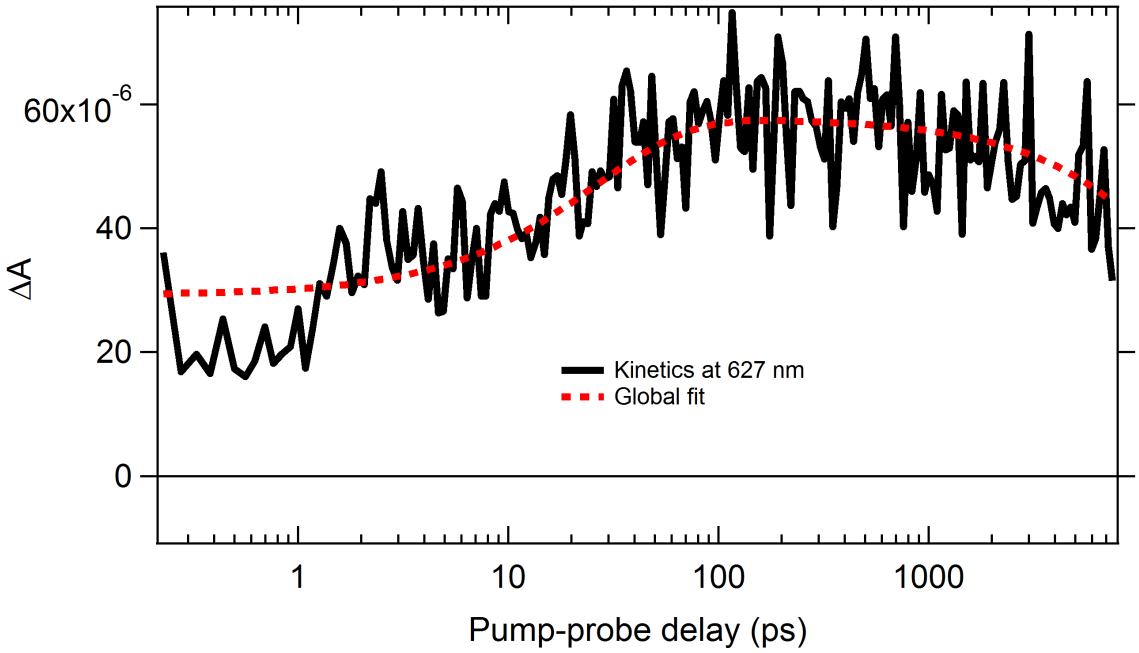

S40. Residual of the above fit with respect to the experimental kinetics.

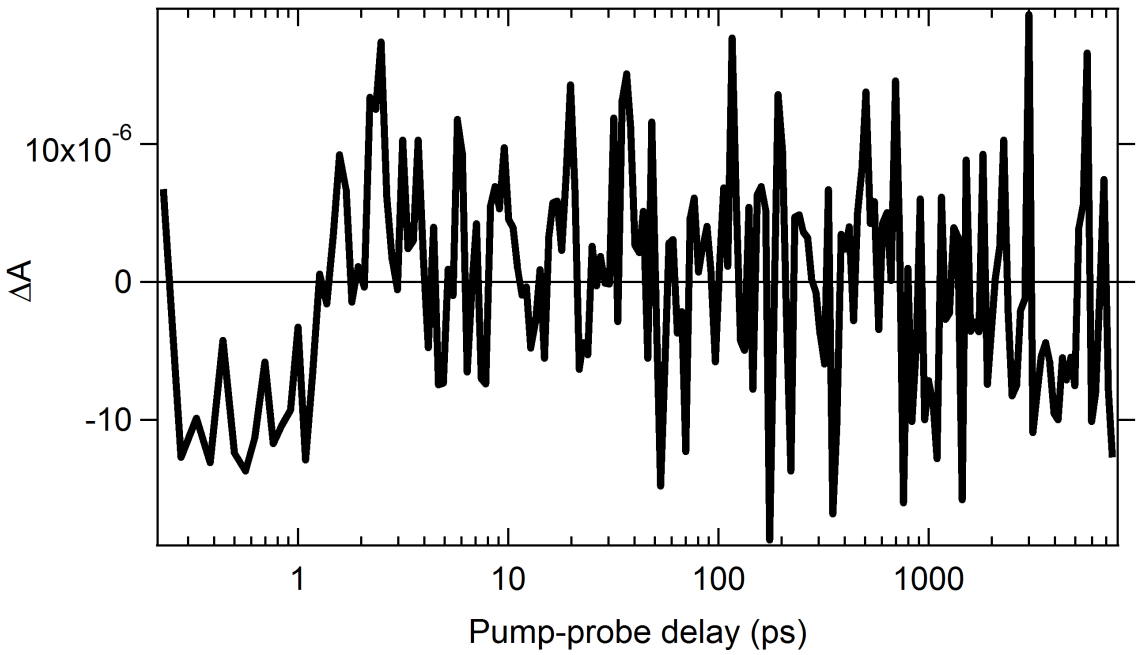

S41. Pump-probe kinetics of the Binary 1 NP solution at 627 nm after photoexcitation at 710 nm with 5 uW pump power, overlayed with a single wavelength trace from the above global fit.

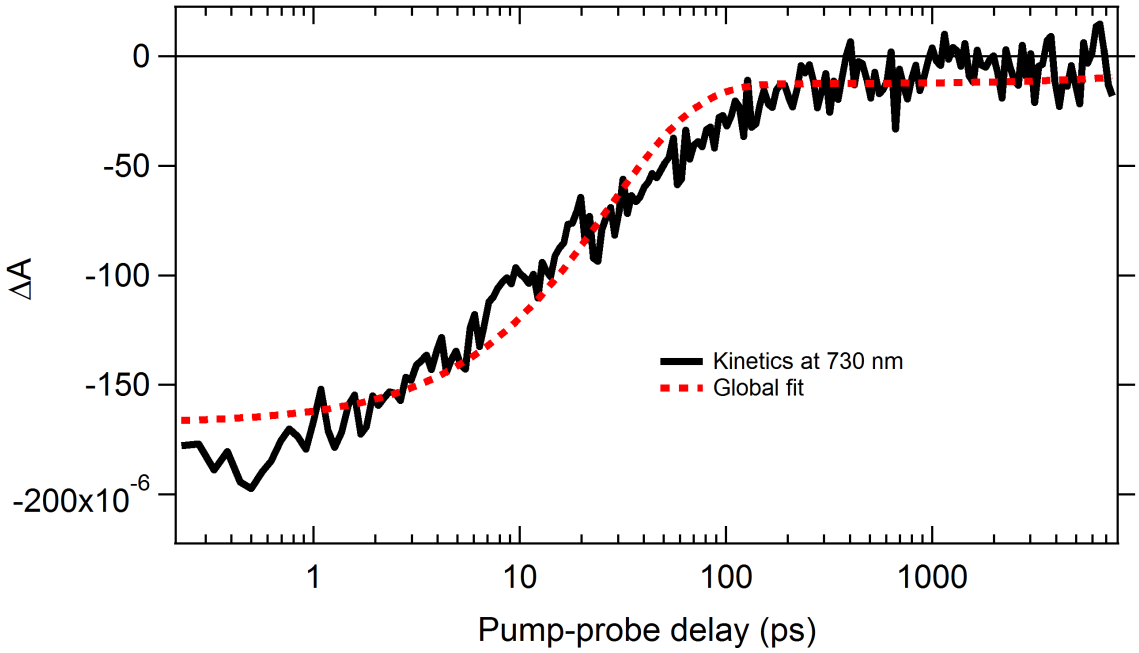

S42. Residual of the above fit with respect to the experimental kinetics.

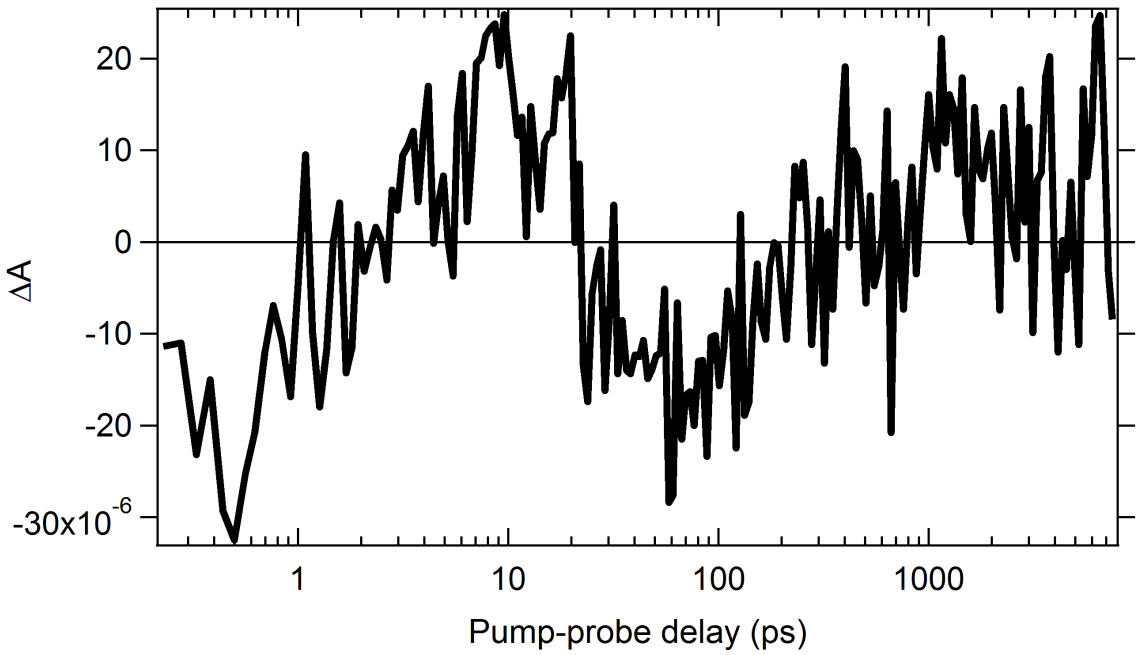

S43. Pump-probe anisotropy at a 710 nm of QDI NP after photoexcitation at 710 nm with 5 uW pump power.

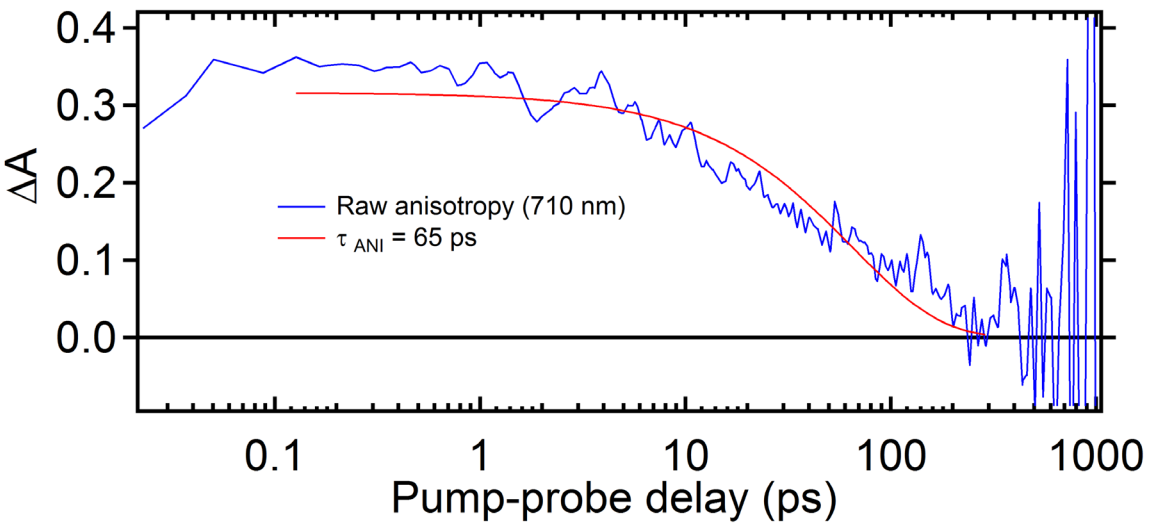

S44. Calculating the ET coupling parameters using Marcus theory

First, in order to get a correct picture of the electron transfer energetics aside from the estimated energy of the QDI exciton, driving force for charge separation can be approximated using the Rehm-Weller equation:

$$\Delta G_{CT} = E_{ox} - E_{red} - E_{QDI} - \frac{e^2}{4\pi r_{DA}\varepsilon\varepsilon_0} + \frac{e^2}{4\pi\varepsilon_0}\left(\frac{1}{2r_D} + \frac{1}{2r_A}\right)\left(\frac{1}{\varepsilon_{ref}} - \frac{1}{\varepsilon}\right)$$

Where E_{ox} and E_{red} are the oxidation and reduction potentials for VONc and QDI respectively as measured by cyclic voltammetry in the reference solvent of dielectric constant ε_{ref}, E_{QDI} is the energy of the lower excitonic excited state of QDI in the nanoparticles, r_{DA} is the estimated intermolecular distance between the radical anion and cation for the QDI-VONc CT state, r_D and r_A are the ionic radii of the ionic species, and ε is the dielectric constant of the nanoparticle, which is estimated to be approximately 3. Using inserting the values for our system into this equation:

$$\Delta G_{CT}(eV) = 1.2\ eV - 1.4\ eV - \frac{e^2}{4\pi(5\ nm)(3)\varepsilon_0} + \frac{e^2}{4\pi\varepsilon_0}\left(\frac{1}{2(1\ nm)} + \frac{1}{2(2\ nm)}\right)\left(\frac{1}{3} - \frac{1}{36.6}\right)$$
$$= \mathbf{-0.30\ eV}$$

The reorganization energy can be calculated according to the Marcus representation using:

$$\lambda(eV) = \frac{e}{4\pi\varepsilon_0}\left(\frac{1}{2r_D} + \frac{1}{2r_A} - \frac{1}{r_{DA}}\right)\left(\frac{1}{n^2} - \frac{1}{\epsilon}\right)$$

Which when we estimate *n* as 3.5 using literature values for a related rylene film(), gives us:

$$\lambda(eV) = \mathbf{0.16\ eV}$$

We can insert these values into the following Marcus theory equation for electron transfer:

$$k_{ET} = \frac{2\pi V_{CT}^2}{\hbar\sqrt{4\pi\lambda k_B T}} \exp(-\frac{\Delta G_{CT} + \lambda}{4\pi\lambda k_B T})$$

Where k_B is the Boltzmann constant and T is the temperature in Kelvin, 298 K. Since all values with the exception of the coupling are known, solving for the positive solution for the coupling gives us:

$$V_{CT} = \mathbf{0.019\ eV}$$

S45. Estimation of the charge transfer efficiency of Binary 1 from pump-probe spectroscopy

We can, however, establish a lower bound on the efficiency of the charge transfer instead by using the results from ultrafast spectroscopy, although this is again complicated by the fact that in Binary 1 there is not only diffusion-limited, but prompt electron transfer from excitons at the interface. We can begin by comparing the time constant of the diffusion-limited charge transfer to the nonradiative decay of the QDI exciton, considering the efficiency of the diffusion limited charge transfer to be:

$$CT\ efficiency\ (diffusion\ limited) = \frac{k_{diffusion-limited\ CT}}{k_{diffusion-limited\ CT} + k_{nonradiative}} \times 100\% = 76\%$$

Considering the added efficiency from prompt charge transfer at the interface is a more complex issue, since it is difficult to assess the number of excitons generated directly at an interface with the VONc. However, we can calculate that if all excitons were generated at an interface and underwent prompt charge transfer, the efficiency as calculated above would be 97%. Now, based on the comparable sizes of the EADS difference spectra shown in figure 4a, we assume that the number of CT events that occurred promptly and diffusion-limited were roughly equal, leading us to the following estimation:

$$\begin{aligned} CT\ efficiency\ (overall) \\ = 0.5 \times CT\ efficiency\ (diffusion\ limited) + 0.5 \\ \times CT\ efficiency\ (prompt) \end{aligned}$$

Leaving us with an overall CT efficiency of approximately 87%. It is important to note that this should not be used with the nanoparticle systems with added polystyrene co-core, since the connectivity of QDI and VONc domains is likely decreased, and hence it is no longer a good assumption to make that the diffusion-limited charge transfer is a possible decay pathway for all generated QDI excitons.

With regards to the comment implying that this would only be of research to a narrow group of researchers, we understand that charge transfer within binary nanoparticles is a relatively narrow field, but this has mostly only been the case because there was such a narrow range of systems that could be made into binary nanoparticle systems, which we combat with our possibly general approach at making binary nanoparticles from small molecular chromophores.